Chemical Science

ROYAL SOCIETY OF CHEMISTRY

EDGE ARTICLE

View Article Online
View Journal | View Issue

Cite this: *Chem. Sci.*, 2025, **16**, 17649

All publication charges for this article have been paid for by the Royal Society of Chemistry

Iminoboronate chemistry enables multifunctional and reprocessable polyphenol-derived vitrimers

Zhan Li,[a] Bo Liang,[b] Rong Zhang,[a] Lei Yang,[a] Xiancheng Ren,[a] Shaohui Xiong,[c] Wei Zhang,[d] Junfei Hu,*[a] Zhipeng Gu *[a] and Yiwen Li *[a]

Received 3rd July 2025
Accepted 14th August 2025

DOI: 10.1039/d5sc04914h

rsc.li/chemical-science

Polyphenol-derived vitrimers offer compelling prospects for sustainable materials owing to their intrinsic recyclability, reprocessability and biodegradability. However, practical development remains constrained by structure degradation under harsh reprocessing conditions and the need for sophisticated modifications of the bio-sourced precursors. Herein, we reported a strategy that integrates commercially available polyphenols and low-molecular-weight PDMS through adaptable iminoboronate chemistry, obviating the need for structural modifications. The N–B coordination lowers the activation barriers for both imine and boronic ester exchange, enabling efficient bond rearrangement. The resulting vitrimers exhibited excellent reprocessability under relatively mild conditions while retaining excellent creep resistance under typical usage conditions. Furthermore, the dynamic chemical framework supports multiple functionalities, including adhesion performance, Fe^{3+}-induced photothermal effects, and anthracene-mediated fluorescence response. Notably, replacing PDMS with a polyurethane matrix yields vitrimers with outstanding mechanical performance (ultimate tensile strength ≈21.4 MPa; elongation at break ≈731%) and enables reprocessing at temperatures as low as 80 °C. This work presents a novel strategy for developing robust and multifunctional vitrimers with mild reprocessing properties, making them suitable for a wide range of practical applications.

Introduction

Vitrimers are polymeric systems featuring dynamic covalent interactions that enable network topology rearrangement and allow adaptation to external stimuli.[1,2] Naturally derived vitrimers have attracted increasing attention due to their potential to reduce carbon footprint, along with desirable properties such as recyclability and mechanical durability.[3] This aligns well with the concept of green and sustainable development.[4–7] The advancement of naturally derived vitrimers can be nicely explained by the proliferation of various adaptive biomass materials, encompassing vitrimers derived from vegetable oils,[8,9] carbohydrates,[10,11] and natural polyphenols.[12,13] This progress also offers promising opportunities for environmentally friendly shape-memory and self-repairing materials.[14,15] However, the reprocessing of vitrimers usually involves high temperatures and pressure conditions, under which biomass materials inevitably undergo oxidation or structural degradation, ultimately compromising material integrity and mechanical performance.[16–18] Therefore, the development of robust and multifunctional naturally derived vitrimers with mild reprocessing capabilities presents both significant importance and considerable challenges.

Associative networks facilitate topology rearrangement in vitrimers while preserving crosslink density. Therefore, in vitrimers systems constructed from oligomeric polymers or small molecule precursors, the relaxation behavior is usually controlled by bond exchange kinetics, as defined by the exchange activation energy (E_a).[19] Lowing E_a enables faster bond rearrangement and facilitates macroscopic flow at the accessible temperature, thereby improving their recyclability and reprocessability.[20] Typically, efficient inorganic and metallic catalysts are used as additives to accelerate the exchange reaction. However, some catalysts, including Brønsted/Lewis acids, strong bases, and transition metals, are frequently associated with toxicity, low compatibility, and catalytic activity towards undesired reactions. These characteristics can adversely impact the mechanical properties of materials and precipitate thermal degradation at elevated temperatures.[21,22] Therefore, utilizing dynamic linkages with intrinsically low E_a is regarded as a promising method for achieving rapid exchange kinetics in vitrimers. Several exchange chemistries, such as

[a]*College of Polymer Science and Engineering, State Key Laboratory of Advanced Polymer Materials, Sichuan University, Chengdu, 610065, China. E-mail: guzhipeng2019@scu.edu.cn; ywli@scu.edu.cn*

[b]*School of Materials Science and Engineering, Hubei University of Automotive Technology, Shiyan 442002, China*

[c]*School of Materials Science and Engineering, Hunan Provincial Key Laboratory of Advanced Materials for New Energy Storage and Conversion, Hunan University of Science and Technology, Xiangtan, 411201, China*

[d]*Department of Pharmaceutical Sciences, University of Pittsburgh, Pittsburgh, Pennsylvania, 15261, USA*

transamination of vinylogous urethanes,[23] diketoenamine exchange,[24] carboxy-exchange by conjugate substitution,[25] *N*,*S*-acetal exchange[26] and addition–elimination reaction of Meldrum's acid,[27] have been successfully implemented to construct fast-relaxing vitrimers. However, the precursors for these reactions usually involve complex modifications to ensure they can form dynamic networks with low E_a. Such modifications are challenging for bio-sourced precursors, which have limited preprocessing methods, such as carboxyl[28,29] and epoxy functionalization.[12,30] Consequently, finding effective ways to integrate commercially available and naturally occurring molecules with adaptable dynamic linkages is crucial to advancing mild and scalable vitrimers systems.

In this work, we selected natural polyphenols for fabricating multifunctional vitrimers since they possess reactive catechol groups and can serve as hydrogen bond donors.[31–33] We constructed a cross-linked network utilizing iminoboronates formed from bis amino-terminated polymer [*e.g.* polydimethylsiloxane (PDMS) and polyurethanes (PU)], 2-formylphenylboronic acids (2-FPBA), and natural polyphenols. Iminoboronate chemistry involves both imine bonds and boronic esters located at the ortho position of imines, where the Lewis conjugate (N–B dative bond) can accelerate boronic ester exchange by several orders of magnitude.[34,35] Notably, the formation of boronic esters with catechol could significantly enhance the N–B dative bond strength, thereby promoting the exchange of imine bonds.[36] Therefore, iminoboronate-based vitrimers undergo rapid stress relaxation, which favors the redistribution of chemical linkages within the networks even at a mild temperature. The presence of iminoboronates could also increase the content of imine bonds and boronic esters in vitrimers owing to the enhanced thermodynamic stability,[37] thereby enhancing the mechanical properties of the materials. More interestingly, the resulting vitrimers exhibited excellent UV-shielding performance, making them ideal candidates for UV absorbers. Additionally, the variety of functional groups present in this system, including amino, aldehyde, boronic acid and catechol, provides adaptability for adhesion to different substrates and opens numerous opportunities for the introduction of various functions, such as photothermal and fluorescent responses. Finally, we successfully extended our strategy to other natural polyphenols or extracts and other polymer matrices.

Results and discussion

It is worth noting that flexible PDMS was deliberately employed as a model building block to minimize the influence of T_g and to clearly demonstrate the feasibility of the iminoboronates strategy. Vitrimers derived from tannic acid (TA, the

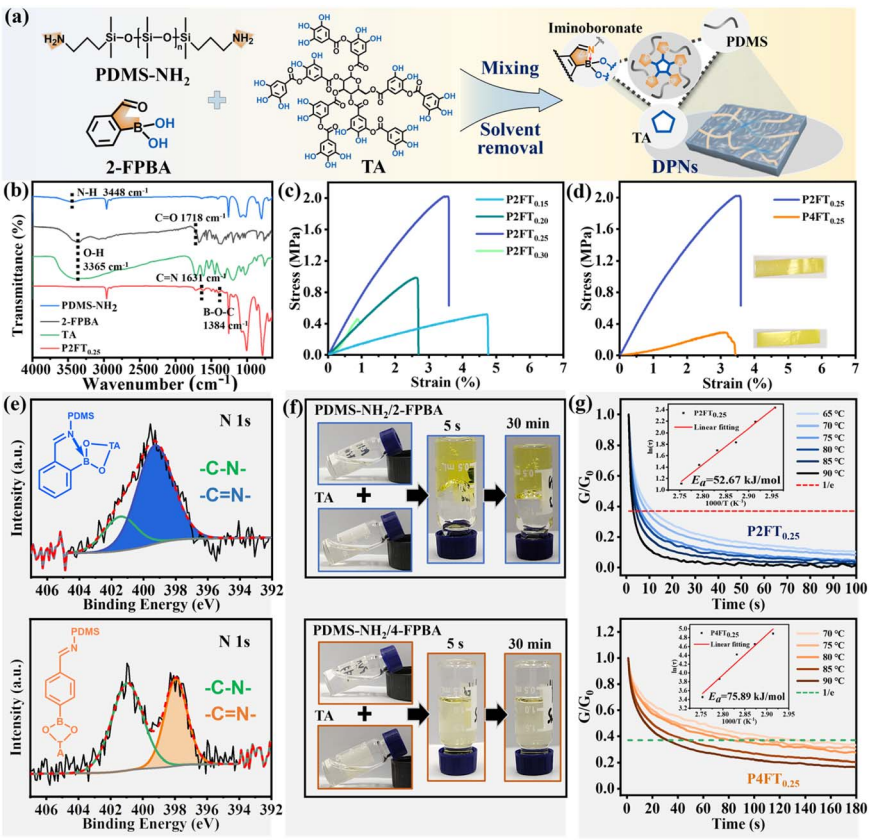

Fig. 1 (a) Schematic representation of the preparation of polyphenol-derived vitrimers *via* simple mixing. (b) FT-IR spectra of PDMS-NH_2, 2-FPBA, TA, and $P2FT_{0.25}$. (c) Stress–strain curves of $P2FT_i$ with different TA content. (d) Stress–strain curves and (e) N 1s high-resolution XPS spectrum of $P2FT_{0.25}$ and $P4FT_{0.25}$. (f) Photo representation of three-component mixing process in anhydrous THF. (g) Stress relaxation plots of $P2FT_{0.25}$ (arrhenius equation, $\ln \tau = 6.33489\ (1000/T) - 16.29361$) and $P4FT_{0.25}$ (arrhenius equation, $\ln \tau = 9.12774\ (1000/T) - 21.60015$).

representative of natural polyphenols) were facilely obtained through directly mixing PDMS-NH_2, 2-FPBA and TA, followed by complete solvent removal (Fig. 1a). It is noteworthy that 5 vt% water was introduced into the system to avoid the formation of an organic gel. The subsequent slow evaporation of the solvent facilitated the formation of a more uniform network and enable direct molding of the vitrimers. Four types of vitrimers consisted of 2-FPBA with different TA content [named $P2FT_i$ (PDMS-NH_2 : 2-FPBA : TA = 1 : 2 : i, n/n, i = 0.15, 0.20, 0.25, and 0.30)] and vitrimers consisted of 4-formylbenzeneboronic acid (4-FPBA) (named $P4FT_{0.25}$) were prepared. FT-IR analysis of the $P2FT_i$ samples showed the disappearance of the C=O stretching vibration peaks at 1718 cm^{-1}, and the emergence of the C=N stretching vibration peaks at 1631 cm^{-1} and the boronic ester (B–O–C) bonds signal peak at 1384 cm^{-1}, suggesting the formation of iminoboronates (Fig. 1b). The optimized TA content was determined through the tensile test of $P2FT_i$. $P2FT_{0.25}$ exhibited the best mechanical properties and was selected for further investigation (Fig. 1c and Table S1). In addition, the mechanical properties of the vitrimers can also be adjusted by using PDMS with different molecular weights (Fig. S1 and Table S2), low molecular weight PDMS increases stiffness but lowers elasticity, while high molecular weight PDMS does the opposite. Note that the stiffness of $P2FT_{0.25}$ was 5 times higher than that of $P4FT_{0.25}$ with the same TA content (Fig. 1d), which may be attributed to the more iminoboronates within the $P2FT_{0.25}$. This assumption was confirmed by the integration ratio of unreacted aldehyde signals (–CHO) observed in ^1H NMR results of the vitrimers analogue composition containing 2-/4-FPBA, TA and small molecule *n*-pentylamine (Fig. S2). X-ray photoelectron spectroscopy (XPS) characterization was performed to investigate the composition of the chemical linkages. In detail, the 1s peak of nitrogen (N 1s) of $P2FT_{0.25}$ mainly consisted of two peaks: C–N at 401.4 eV and C=N at 399.3 eV, as well as the 1s peak of nitrogen (N 1s) of $P4FT_{0.25}$ mainly consisted of two peaks: C–N at 401.0 eV and C=N at 398.0 eV (Fig. 1e). Notably, the C=N peak of $P2FT_{0.25}$ exhibited a higher shift in binding energy compared to $P4FT_{0.25}$, which may be attributed to the intramolecular N–B coordination present in $P2FT_{0.25}$. Furthermore, a higher content of imine and boronic ester was also confirmed in $P2FT_{0.25}$, which can be credited to the thermodynamic stability provided by iminoboronates (Fig. 1e and S3). The reaction kinetics of iminoboronates were further demonstrated by three-component mixing experiments in anhydrous THF. As shown in Fig. 1f, the $P2FT_{0.25}$ started to form organic gel in 5 seconds and complete in 30 minutes, while $P4FT_{0.25}$ remained liquid-like. We further explored the dynamic viscoelastic properties of $P2FT_{0.25}$ and $P4FT_{0.25}$. The oscillatory strain sweep revealed that the intersection points of storage modulus (G') and loss modulus (G'') were at the strain of 48.6% for $P2FT_{0.25}$ and 9.5% for $P4FT_{0.25}$, illustrating that the chemical connections in $P2FT_{0.25}$ internal network are more stable (Fig. S4b and e). Both $P2FT_{0.25}$ and $P4FT_{0.25}$ exhibited a constant rubbery plateau in the temperature sweep experiments. The cross-linking density, as determined from the modulus, further suggested that $P2FT_{0.25}$ performed a densely cross-linking network (Fig. S4c, f and Table S3). In addition, the darkening of the color of $P4FT_{0.25}$ after heating also indicated that a large amount of exposed catechol was oxidized, while $P2FT_{0.25}$ remained unchanged. Stress relaxation measurements were carried out to study the associative exchange mechanism of $P2FT_{0.25}$ and $P4FT_{0.25}$ (Fig. 1g). Their relaxation time showed the characteristic of decreasing with the increase of temperature, which can be attributed to imine exchange, boronic ester exchange, and hydrogen bond dissociation. Although $P2FT_{0.25}$ has a higher cross-linking density, its relaxation time (8.9 s, 70 °C) was significantly shortened compared to $P4FT_{0.25}$ (133.5 s, 70 °C). And then the E_a of $P2FT_{0.25}$ and $P4FT_{0.25}$ were calculated to be 52.67 and 75.89 kJ mol^{-1}, respectively, using the Arrhenius equation derived from the temperature dependence of relaxation times. This substantial difference primarily in E_a is attributed to the synergistic effect of the iminoboronate structure in $P2FT_{0.25}$, which simultaneously lowers the activation barriers for both imine and boronic ester exchange, thereby significantly accelerating network reconfiguration.

Next, the dynamic exchange capability of $P2FT_{0.25}$ was evaluated. As shown in Fig. 2a, the material exhibited efficient scratch healing without applied stress, and mechanical testing confirmed a self-healing efficiency of up to 85% (Fig. S5). To evaluate the reprocessability of $P2FT_{0.25}$, compression molding was conducted. As shown in Fig. 2b, small pieces of $P2FT_{0.25}$ can be perfectly remolded under a pressure of 1 MPa at 40 °C, attributed to the low associative exchange E_a of iminoboronates within the macromolecular networks. In contrast, $P4FT_{0.25}$ remains unprocessable under the same conditions, highlighting the critical role of network dynamics in reprocessability. Further investigation about the effects of pressure and holding time showed that $P2FT_{0.25}$ could be reshaped under relatively mild conditions, requiring only 1 MPa of pressure for 5 minutes (Fig. S6 and Table S4). Moreover, the material's Young's modulus, elongation at break, and tensile strength remain almost identical to those of the original material after three cycles, indicating excellent recovery stability (Fig. 2c and Table S5). UV-vis spectroscopy analysis further showed that the transparency of the films remained essentially unchanged after three cycles, indicating that catechol was not oxidized (Fig. 2d). Fig. 2e and Table S6 demonstrated that the reprocessing temperature and time of vitrimers composed of iminoboronates were far below those of vitrimers during the recent years.[23,25–27,38–47] Although the rapid exchange of dynamic bonds may compromise the long-term dimensional stability of the material, it is noteworthy that $P2FT_{0.25}$ exhibits substantially lower irreversible deformation than $P4FT_{0.25}$. This phenomenon can be attributed to the higher thermodynamic stability of iminoboronate, which enables the formation of a more densely crosslinked network in $P2FT_{0.25}$, thereby exhibiting better creep resistance (Fig. 2f and Table S3). Moreover, the solvent resistance of the films was assessed by swelling experiments (Fig. S7). The hydrophobicity of PDMS allows the films to maintain a complete three-dimensional network structure in water. However, the chemical equilibrium of iminoboronates in the cross-linking network can be interrupted when a small amount of water was added to the THF-swollen film, thereby

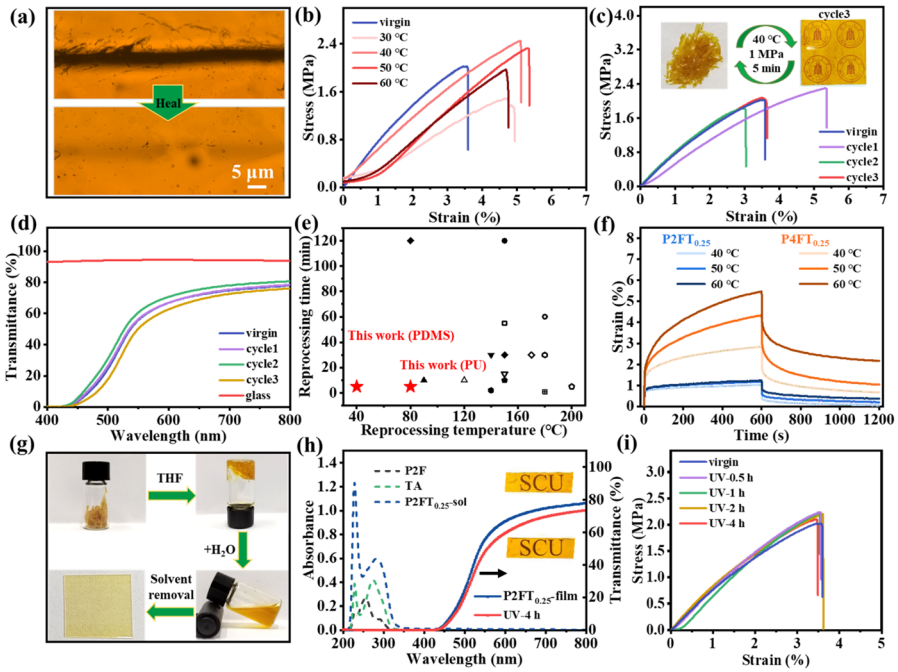

Fig. 2 Physical properties of $P2FT_{0.25}$. (a) Photos of the scratched $P2FT_{0.25}$ film treated at 100 °C for 1 h. (b) Stress–strain curves of $P2FT_{0.25}$ reprocessing at different temperature. (c) Stress–strain curves of $P2FT_{0.25}$ for different recycling cycle. (d) Visible light spectra of glass and $P2FT_{0.25}$ film with different recycling cycle. (e) Comparison of $P2FT_{0.25}$ and other vitrimers in terms of reprocessing temperature and time. (f) Creep experiment plots of $P2FT_{0.25}$ and $P4FT_{0.25}$. (g) Recycling process of $P2FT_{0.25}$ (thickness: 170 μm). (h) UV-vis spectra of P2F (PDMS-NH_2 and 2-FPBA), TA, $P2FT_{0.25}$ solution, $P2FT_{0.25}$ film (thickness: 500 μm), and $P2FT_{0.25}$ film irradiated by UV for 4 h. (i) Stress–strain curves of $P2FT_{0.25}$ film irradiated by UV for different time.

enabling films recycling. After the solvent was completely evaporated, the iminoboronates would be regenerated to obtain the yellow $P2FT_{0.25}$ (Fig. 2g). As most catechol moieties participate in the formation of iminoboronate linkages, this dynamic bonding configuration effectively protects them from UV-induced oxidation. Only a small fraction of unbound phenolic hydroxyl groups undergoes slight oxidation upon UV exposure, leading to minor fluctuations in the UV absorption of the vitrimers. This finding indicates the excellent UV stability and shielding capability of $P2FT_{0.25}$ (Fig. 2h). The transparency and mechanical properties of the films remained unchanged after exposure to UV light for 4 h, suggesting that the films have the potential to serve as UV-shielding materials (Fig. 2i and Table S7). The free radical scavenging ability of the films was investigated using an $ABTS^{\cdot+}$ free radical scavenging experiment. Fig. S8 showed a positive correlation between film weight and free radical scavenging capacity, suggesting the existence of trace amounts of unbound phenolic hydroxyl groups within the network. To further evaluate the thermal stability of the films, thermogravimetric analysis (TGA) and differential scanning calorimetry (DSC) were conducted. The results indicated that the stability of cross-linked networks and the multiple hydrogen bonding interactions between polyphenols significantly improved the thermal stability of the polymers (Fig. S9 and S10).

Owing to the presence of chemically active groups within the polymer network, including catechol, boronic acid, amino, and aldehyde groups, $P2FT_{0.25}$ can effectively generate adhesion to diverse substrates *via* hierarchical interfacial interactions. To evaluate its adhesion performance, $P2FT_{0.25}$ was applied either directly (Method 1) or in a THF-swollen state (Method 2) as a glue between various substrates, followed by thermal curing at 100 °C for 30 minutes. Upon heating, the dynamic bond exchange kinetics were accelerated and hydrogen bonds were disrupted, enabling $P2FT_{0.25}$ to form robust interfacial bridges with the substrate surface through various interactions. As shown in Fig. 3a and b, lap shear testing of neat $P2FT_{0.25}$ (Method 1) demonstrated excellent bonding ability to wood (1.35 ± 0.08 MPa), glass (0.71 ± 0.11 MPa), PET (0.48 ± 0.02 MPa), Cu (0.25 ± 0.07 MPa), Fe (0.47 ± 0.08 MPa), Al (0.87 ± 0.07 MPa), and steel (1.14 ± 0.08 MPa). For wood and PET, hydrogen bonding likely dominates the interfacial interactions, while π–π and cation–π interactions between $P2FT_{0.25}$ and wood may further enhance adhesion. B–O and hydrogen bonding served as a source of adhesion for hydroxyl group terminated materials (glass, Al, and steel). In addition, the coordination between polyphenols and metal elements also contributed to the adhesion of $P2FT_{0.25}$ to metal substrates. The incorporation of high-density dynamic bonds and their rapid reorganization under thermal activation facilitated network optimization and enhanced interfacial wettability. As a result, $P2FT_{0.25}$ showed no significant performance degradation after five adhesion cycles, demonstrating excellent reusability (Fig. 3c). And $P2FT_{0.25}$ still maintained good adhesion strength after one month of storage under 80% relative humidity, attributed to the hydrophobicity of PDMS (Fig. 3d). Unsurprisingly, $P2FT_{0.25}$-adhered wood could easily hang a 20 kg bucket

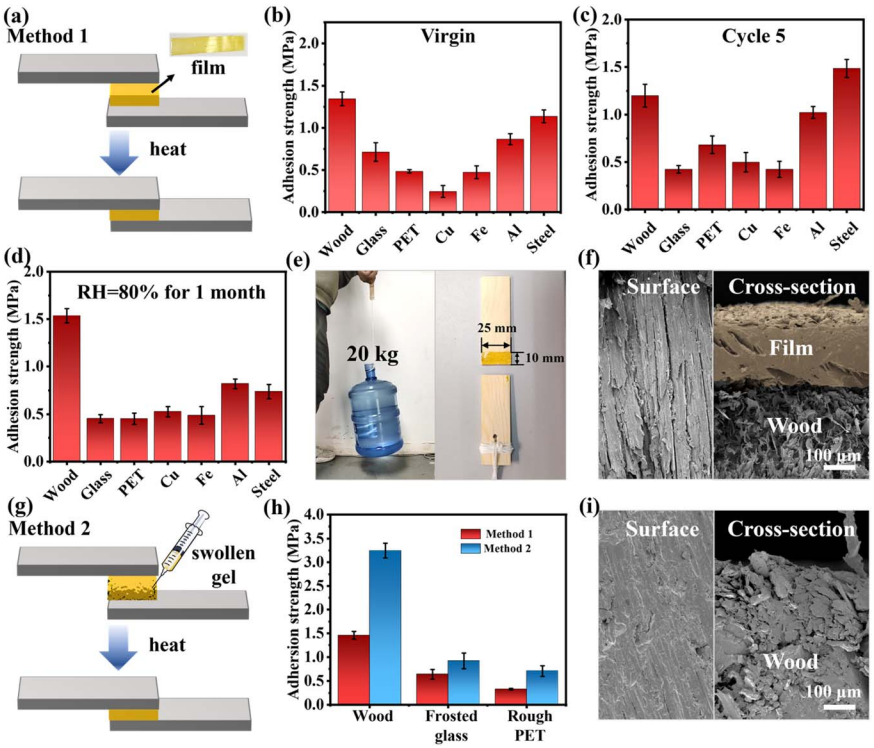

Fig. 3 Adhesion of P2FT$_{0.25}$. (a) Schematic representation of the P2FT$_{0.25}$ film adhesive procedure. Adhesive strengths of the P2FT$_{0.25}$ film to various substrates under (b) 0 cycle and (c) 5th cycle. (d) Adhesive strengths of the P2FT$_{0.25}$ film to various substrates at a relative humidity of 80% for 1 month. (e) The P2FT$_{0.25}$ film adhered between two wood substrates and supported a load of 20 kg. (f) Surface and cross section SEM images of fractured samples in Method 1. (g) Schematic representation of the P2FT$_{0.25}$ swollen gel adhesive procedure. (h) Comparison of adhesion strength of two methods to rough substrate. (i) Surface and cross section SEM images of fractured samples in Method 2.

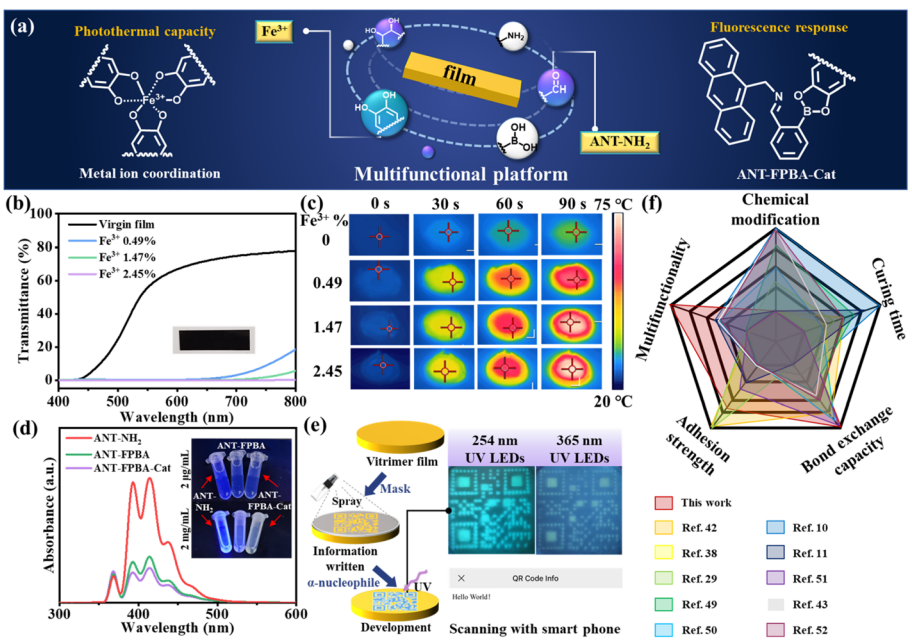

Fig. 4 Multifunctions of P2FT$_{0.25}$. (a) Schematic illustration of the P2FT$_{0.25}$ film as a multifunctional platform that can incorporate metal ions and fluorescent molecules. (b) Visible light spectra of P2FT$_{0.25}$ film with different Fe^{3+} content. (c) IR image of P2FT$_{0.25}$ film with different Fe^{3+} content under two sun for 90 s. (d) The fluorescence spectra of ANT-NH$_2$, ANT-FPBA, and ANT-FPBA-Cat (excitation wavelength: 370 nm). The insets are images of ANT-NH$_2$, ANT-FPBA, and ANT-FPBA-Cat with different concentrations under 365 nm UV LEDs. (e) Schematic diagram of information encryption and decryption. (f) Comparison of multifunctional polyphenol-derived adhesives with other naturally derived vitrimers.

without damage (Fig. 3e). To elucidate the failure modes in the adhered wood in Method 1, SEM imaging of $P2FT_{0.25}$-adhered wood surfaces and cross-sections was conducted (Fig. 3f). The images revealed rough, damaged wood surfaces, indicating interfacial adhesive failure. Notably, the THF-swollen $P2FT_{0.25}$ exhibits markedly enhanced surface conformability and penetration due to its increased fluidity, yielding superior adhesion on rough substrates. This effect is especially pronounced on wood, where the porous microstructure facilitates deeper adhesive infiltration, resulting in a threefold increase in shear strength (3.25 ± 0.16 MPa) (Fig. 3g and h). SEM analysis of the failed wood interface from Method 2 (Fig. 3i) revealed smooth fracture surfaces, consistent with cohesive failure within the adhesive layer.

The abundant chemical groups within the polymer networks provides the potential for employing $P2FT_{0.25}$ to robustly and easily construct a variety of multifunctional modules through dynamic linkages. As depicted in Fig. 4a, Fe^{3+} ions were simply incorporated into the polymer architecture to endow the film with photothermal responsiveness. In detail, the visible light transmittance of the vitrimers decreased rapidly with the increase of Fe^{3+} content, which might be due to the coordination of TA and Fe^{3+} ions could lead to an increase in visible light absorption (Fig. 4b and S11). Benefiting from the promising photothermal properties of TA/Fe^{3+} chelates,[48] the temperature of vitrimers incorporating 2.45% Fe^{3+} rose rapidly to ~75 °C within 90 s under two-sun illumination. In contrast, the temperature of the pure film rose to 44 °C due to limited visible light absorption (Fig. 4c and S12). Although the light-induced heating can cover the processing temperature range of $P2FT_{0.25}$, its associative exchange mechanism effectively maintains the structural stability of the materials during bond exchange, offering substantial advantage for its application in photothermal conversion.

Another interesting example involves the fluorescence quenching observed upon formation of an imine between florescent anthracene-9-ylmethanamine (ANT-NH_2) and FPBA (Fig. 4a, right). This quenching is likely attributed to the electron-donating effect of the imine linkage, which enhances photoinduced electron transfer (PET) quenching from the anthracene moiety (Fig. 4d). Subsequent reaction with catechol (Cat) promotes the formation of N–B coordination, thereby disrupting the PET pathway and restoring fluorescence. However, the red-shifted absorption of catechol–boronic ester complexes partially overlaps with both the excitation and emission wavelengths of ANT, leading to modest decrease in fluorescence

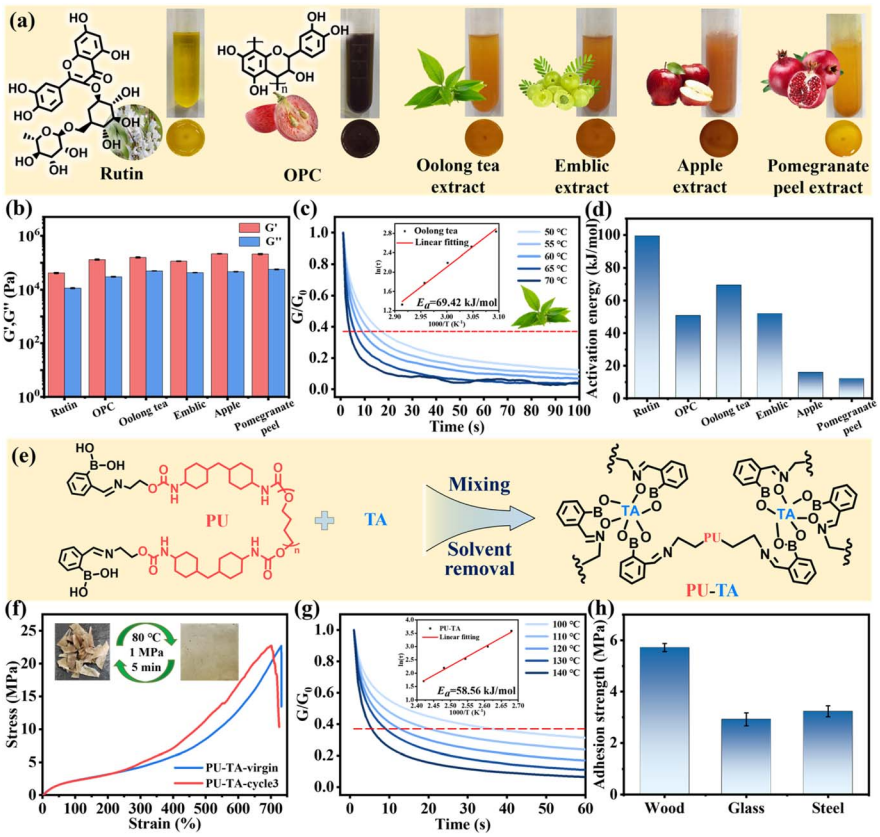

Fig. 5 Preparation of various vitrimers. (a) Structure diagram of natural polyphenols, the inserts are optical images of three-component mixture and dried films from different polyphenols. (b) The storage modulus (G') and the loss modulus (G'') of different vitrimers. These studies were carried out conducted at 0.1% strain and an angular frequency of 1 Hz. (c) Stress relaxation plots of vitrimers from Oolong tea extract. (d) Activation energy of vitrimers from various polyphenols. (e) Synthesis route of PU-TA. (f) Stress–strain curves, (g) stress relaxation plots and (h) adhesion strength of PU-TA.

intensity in the ANT-FPBA-Cat system. This spectral interference becomes pronounced at elevated catechol concentrations. Utilizing these properties, we fabricated fluorescent vitrimers suitable for information security applications (Fig. 4e). The resulting film remains stable under aqueous and mildly acid conditions due to the intrinsic hydrophobicity of PDMS. Upon exposure to nucleophilic stimuli, ANT-NH_2 was released, recovering its fluorescence (Fig. S13). This straightforward and versatile strategy for functional integration renders $P2FT_{0.25}$ films an attractive multifunctional platform for stimulus-responsive systems. To illustrate the exceptional properties of the $P2FT_{0.25}$, we summarized some of the key parameters on naturally derived vitrimers in recent years, including chemical modification, curing time, bond exchange capacity, adhesion capacity and multifunctionality (Fig. 4f).[10,11,29,38,42,43,49–52] Notably, the $P2FT_{0.25}$ vitrimers is readily fabricated without the need for additional chemical modifications and boasts an extremely short curing time. The distinctive N–B coordination mechanism enabled $P2FT_{0.25}$ to possess a significantly lower activation energy (52.67 kJ mol^{-1}) for chemical bond exchange compared to most ester-exchange based vitrimers (>100 kJ mol^{-1}). Furthermore, the abundance of functional moieties within $P2FT_{0.25}$ enables adhesion to diverse substrates and facile incorporation of responsive functionalities.

Considering the structural similarities among various nature polyphenols and their extracts, the design principles of $P2FT_{0.25}$ can be easily expanded to other polyphenol-based vitrimers in a modular manner. To validate this concept, rutin, oligometric proanthocyanidins (OPC), and a series of polyphenol-containing extracts (*e.g.* Oolong tea, emblic, apple, and pomegranate peel) were selected as polyphenol building blocks to prepare the vitrimers. As shown in Fig. 5a, six additional polyphenol-derived vitrimers were successfully prepared. The activation energies of these materials were calculated to be 99.43, 50.83, 69.42, 51.95, 15.96, and 12.13 kJ mol^{-1}, respectively. These differences are primarily attributed to variations in the proportions of dynamic iminoboronates and hydrogen bonding within the crosslinked networks formed by different polyphenols (Fig. 5b–d and S14). Notably, recognizing the critical role of the polymer matrix in governing material properties, we synthesized polyurethane end-capped with 2-FPBA (PU) and incorporated TA to construct PU-TA vitrimers for further validating the universality of our strategy (Fig. 5e and S15). The resulting material exhibited outstanding mechanical performance (ultimate tensile strength ≈21.4 MPa; elongation at break ≈731%) while enabling reprocessing at temperatures as low as 80 °C (Fig. 5f and Table S8). Under the same conditions, vitrimers without polyphenols cannot be reprocessed at 80 °C (Fig. S16). Moreover, PU-TA exhibited rapid stress relaxation (36 s at 100 °C), a low activation energy (58.56 kJ mol^{-1}), and strong substrate adhesion to various substrates (Fig. 5g and h). These findings indicate that iminoboronate chemistry can effectively balance the mechanical performance and mild reprocessability of vitrimers. Therefore, the strategy of integrating natural polyphenols with iminoboronate chemistry presented a robust and generalizable platform for developing multifunctional natural-derived vitrimers.

Conclusions

In summary, we have successfully developed an iminoboronate strategy to prepare multifunctional polyphenol-derived vitrimers with mild reprocessing temperatures. The high dynamicity of the iminoboronates facilitates the redistribution of macromolecular networks under mild conditions, enabling the rapid reprocessing of vitrimers without generating side reactions or material changes. Owing to the inherent reactivity of iminoboranates, the integration of unmodified natural polyphenols into polymer matrices is facile and efficient. The high cross-linking density imparted by iminoboronates enables these vitrimers to maintain dimensional stability. Certainly, a more rigid backbone can be designed to further balance creep resistance and processability. Alternatively, in the presence of water, the iminoboronate-based associative vitrimers described in this study may undergo partial transformation into dissociative vitrimers. Although dissociation is enthalpically unfavorable, these vitrimers exhibit relatively low activation energy barriers. This transformation could enable the realization of highly dynamic vitrimers with negligible creep.[53] Crucially, the existence of abundant dynamic chemical bonds within the polymer networks, including hydrogen bonds, imine bonds, and boronic esters, provides a robust chemical foundation for vitrimers as an adhesive and multifunctional platform. We believe this work presents a valuable chemical strategy for designing robust, reprocessable, and multifunctional vitrimers derived from natural sources, with great potential for applications in energy dissipation and electronic sensing.

Author contributions

Z. L., J. H. and Y. L. conceived the idea and designed the study. Z. L. and J. H. performed the experiments. Z. L. and B. L. analyzed the results. Z. L., J. H., Z. G. and Y. L. wrote and refined the paper. R. Z., L. Y., X. R., S. X., W. Z. and Z. G. help design and discussed the experiments. All authors contributed to the discussion of the manuscript.

Conflicts of interest

There are no conflicts to declare.

Data availability

The data supporting this article have been included as part of the SI. See DOI: **https://doi.org/10.1039/d5sc04914h**.

Acknowledgements

This work was supported by the National Natural Science Foundation of China (52303377 and 52225311), Sichuan Science and Technology Program (2025ZNSFSC1393), China Postdoctoral Science foundation (2023M742444), State Key Laboratory of Advanced Polymer Materials, Sichuan University (sklpme2024-2-07), the Science and Technology Innovation Program of Hunan Province (2024RC4007). We acknowledge the

help of Dandan Yuan from the College of Polymer Science and Engineering at Sichuan University for rheological testing.

References

1 A. M. Wemyss, C. Ellingford, Y. Morishita, C. Bowen and C. Wan, *Angew. Chem., Int. Ed.*, 2021, **60**, 13725–13736.
2 M. J. Webber and M. W. Tibbitt, *Nat. Rev. Mater.*, 2022, **7**, 541–556.
3 C. Cui, F. Wang, X. Chen, T. Xu, Z. Li, K. Chen, Y. Guo, Y. Cheng, Z. Ge and Y. Zhang, *Adv. Funct. Mater.*, 2024, **24**, 2315469.
4 M. A. Lucherelli, A. Duval and L. Avérous, *Prog. Polym. Sci.*, 2022, **127**, 101515.
5 T. Vidil and A. Llevot, *Macromol. Chem. Phys.*, 2022, **223**, 2100494.
6 L. Zhang, J. Liang, C. Jiang, Z. Liu, L. Sun, S. Chen, H. Xuan, D. Lei, Q. Guan, X. Ye and Z. You, *Natl. Sci. Rev.*, 2020, **8**, nwaa154.
7 S.-S. Wu, H.-J. Lu, Y.-D. Li, S.-D. Zhang and J.-B. Zeng, *Chin. J. Polym. Sci.*, 2024, **42**, 1414–1424.
8 F. I. Altuna, V. Pettarin and R. J. J. Williams, *Green Chem.*, 2013, **15**, 3360–3366.
9 J. Wu, X. Yu, H. Zhang, J. Guo, J. Hu and M.-H. Li, *ACS Sustain. Chem. Eng.*, 2020, **8**, 6479–6487.
10 W. Zhao, Z. Feng, Z. Liang, Y. Lv, F. Xiang, C. Xiong, C. Duan, L. Dai and Y. Ni, *ACS Appl. Mater. Interfaces*, 2019, **11**, 36090–36099.
11 F. Lossada, J. Guo, D. Jiao, S. Groeer, E. Bourgeat-Lami, D. Montarnal and A. Walther, *Biomacromolecules*, 2019, **20**, 1045–1055.
12 S. Zhao and M. M. Abu-Omar, *Macromolecules*, 2019, **52**, 3646–3654.
13 Y. Tao, L. Fang, M. Dai, C. Wang, J. Sun and Q. Fang, *Polym. Chem.*, 2020, **11**, 4500–4506.
14 P. Li, X. Zhang, Q. Yang, P. Gong, C. B. Park and G. Li, *J. Mater. Chem. A*, 2023, **11**, 10912–10926.
15 J. Zheng, Z. M. Png, S. H. Ng, G. X. Tham, E. Ye, S. S. Goh, X. J. Loh and Z. Li, *Mater. Today*, 2021, **51**, 586–625.
16 D. J. Fortman, J. P. Brutman, C. J. Cramer, M. A. Hillmyer and W. R. Dichtel, *J. Am. Chem. Soc.*, 2015, **137**, 14019–14022.
17 Z. Yang, F. Wang, C. Zhang, J. Li, R. Zhang, Q. Wu, T. Chen and P. Sun, *Polym. Chem.*, 2019, **10**, 3362–3370.
18 J. Hu, L. Yang, P. Yang, S. Jiang, X. Liu and Y. Li, *Biomater. Sci.*, 2020, **8**, 4940–4950.
19 G. M. Scheutz, J. J. Lessard, M. B. Sims and B. S. Sumerlin, *J. Am. Chem. Soc.*, 2019, **141**, 16181–16196.
20 R. Hajj, A. Duval, S. Dhers and L. Avérous, *Macromolecules*, 2020, **53**, 3796–3805.
21 F. Cuminet, S. Caillol, É. Dantras, É. Leclerc and V. Ladmiral, *Macromolecules*, 2021, **54**, 3927–3961.
22 D. Berne, F. Cuminet, S. Lemouzy, C. Joly-Duhamel, R. Poli, S. Caillol, E. Leclerc and V. Ladmiral, *Macromolecules*, 2022, **55**, 1669–1679.
23 F. Van Lijsebetten, K. De Bruycker, Y. Spiesschaert, J. M. Winne and F. E. Du Prez, *Angew. Chem., Int. Ed.*, 2022, **61**, e202113872.
24 P. R. Christensen, A. M. Scheuermann, K. E. Loeffler and B. A. Helms, *Nat. Chem.*, 2019, **11**, 442–448.
25 N. Nishiie, R. Kawatani, S. Tezuka, M. Mizuma, M. Hayashi and Y. Kohsaka, *Nat. Commun.*, 2024, **15**, 8657.
26 T. Habets, G. Seychal, M. Caliari, J.-M. Raquez, H. Sardon, B. Grignard and C. Detrembleur, *J. Am. Chem. Soc.*, 2023, **145**, 25450–25462.
27 J. S. A. Ishibashi and J. A. Kalow, *ACS Macro Lett.*, 2018, **7**, 482–486.
28 C. Hao, T. Liu, S. Zhang, L. Brown, R. Li, J. Xin, T. Zhong, L. Jiang and J. Zhang, *ChemSusChem*, 2019, **12**, 1049–1058.
29 S. Zhang, T. Liu, C. Hao, L. Wang, J. Han, H. Liu and J. Zhang, *Green Chem.*, 2018, **20**, 2995–3000.
30 T. Liu, C. Hao, S. Zhang, X. Yang, L. Wang, J. Han, Y. Li, J. Xin and J. Zhang, *Macromolecules*, 2018, **51**, 5577–5585.
31 Y. Xu, J. Hu, J. Hu, Y. Cheng, X. Chen, Z. Gu and Y. Li, *Prog. Polym. Sci.*, 2023, **146**, 101740.
32 T. Wang, J. Zhao, Z. Yang, L. Xiong, L. Li, Z. Gu and Y. Li, *Green Chem.*, 2022, **24**, 3605–3622.
33 P. Yang, J. Zhang, R. Zhang, G. Duan, Y. Li and Z. Li, *Green Chem.*, 2024, **26**, 3329–3337.
34 S. Cambray and J. Gao, *Acc. Chem. Res.*, 2018, **51**, 2198–2206.
35 S. Chatterjee, E. V. Anslyn and A. Bandyopadhyay, *Chem. Sci.*, 2021, **12**, 1585–1599.
36 J. Hu, L. Li, Z. Li, L. Yang, X. Ren, Y. Cheng, Y. Li and Q. Huang, *Adv. Funct. Mater.*, 2024, **34**, 2411234.
37 A. Bandyopadhyay and J. Gao, *J. Am. Chem. Soc.*, 2016, **138**, 2098–2101.
38 S. Dhers, G. Vantomme and L. Avérous, *Green Chem.*, 2019, **21**, 1596–1601.
39 X. Zhang, S. Wang, Z. Jiang, Y. Li and X. Jing, *J. Am. Chem. Soc.*, 2020, **142**, 21852–21860.
40 J. Joe, J. Shin, Y.-S. Choi, J. H. Hwang, S. H. Kim, J. Han, B. Park, W. Lee, S. Park, Y. S. Kim and D.-G. Kim, *Adv. Sci.*, 2021, **8**, 2103682.
41 A. Ruiz de Luzuriaga, R. Martin, N. Markaide, A. Rekondo, G. Cabañero, J. Rodríguez and I. Odriozola, *Mater. Horiz.*, 2016, **3**, 241–247.
42 A. Moreno, M. Morsali and M. H. Sipponen, *ACS Appl. Mater. Interfaces*, 2021, **13**, 57952–57961.
43 L. Zhong, Y. Hao, J. Zhang, F. Wei, T. Li, M. Miao and D. Zhang, *Macromolecules*, 2022, **55**, 595–607.
44 M. Röttger, T. Domenech, R. van der Weegen, A. Breuillac, R. Nicolaÿ and L. Leibler, *Science*, 2017, **356**, 62–65.
45 T. Debsharma, V. Amfilochiou, A. A. Wróblewska, I. De Baere, W. Van Paepegem and F. E. Du Prez, *J. Am. Chem. Soc.*, 2022, **144**, 12280–12289.
46 Y. Spiesschaert, M. Guerre, I. De Baere, W. Van Paepegem, J. M. Winne and F. E. Du Prez, *Macromolecules*, 2020, **53**, 2485–2495.
47 C.-B. Zhao, L.-K. Feng, H. Xie, M.-L. Wang, B. Guo, Z.-Y. Xue, C.-Z. Zhu and J. Xu, *Chin. J. Polym. Sci.*, 2024, **42**, 73–86.
48 M. Li, H. Wang, J. Hu, J. Hu, S. Zhang, Z. Yang, Y. Li and Y. Cheng, *Chem. Mater.*, 2019, **31**, 7678–7685.
49 M. Thys, J. Brancart, G. Van Assche, R. Vendamme and N. Van den Brande, *Macromolecules*, 2021, **54**, 9750–9760.

50 Y.-Y. Liu, G.-L. Liu, Y.-D. Li, Y. Weng and J.-B. Zeng, *ACS Sustain. Chem. Eng.*, 2021, **9**, 4638–4647.
51 J. Hong, Y. Hong, J. Jeong, D. Oh and M. Goh, *ACS Sustain. Chem. Eng.*, 2023, **11**, 14112–14123.
52 Y. Xu, S. Dai, L. Bi, J. Jiang, H. Zhang and Y. Chen, *Chem. Eng. J.*, 2022, **429**, 132518.
53 F. Van Lijsebetten, T. Debsharma, J. M. Winne and F. E. Du Prez, *Angew. Chem., Int. Ed.*, 2022, **61**, e202210405.